PCCP

Cite this: *Phys. Chem. Chem. Phys.*, 2011, **13**, 21451–21460

www.rsc.org/pccp

PAPER

The specific vibrational modes of GTP in solution and bound to Ras: a detailed theoretical analysis by QM/MM simulations†

Fei Xia,[a] Till Rudack,[b] Carsten Kötting,[b] Jürgen Schlitter[b] and Klaus Gerwert*[ab]

Received 26th August 2011, Accepted 12th October 2011
DOI: 10.1039/c1cp22741f

The hydrolysis of guanosine triphosphate (GTP) in general, and especially by GTPases like the Ras protein, is in the focus of biological investigations. A huge amount of experimental data from Fourier-transformed infrared studies is currently available, and many vibrational bands of free GTP, GTP·Mg^{2+}, and Ras·GTP·Mg^{2+} in solution have been assigned by isotopic labeling. In the Ras environment, bands between 800 cm^{-1} and 1300 cm^{-1} have already been assigned, but not those below 800 cm^{-1}. The combination of quantum and molecular mechanics (QM/MM) methods takes the quantum effects for selected relevant atoms into account. This provides structural details, vibrational frequencies and electron distributions of the region of interest. We therefore used MM and QM/MM simulations to investigate the normal vibrational modes of GTP, GTP·Mg^{2+}, and Ras·GTP·Mg^{2+} in solution, and assigned the vibrational frequencies for each normal vibration mode. In this study, the quantum box contains the nucleoside and the Mg^{2+}. The comparison of calculated and experimental vibrational spectra provides a very good control for the quality of the calculations. Structurally, MM and QM/MM simulations reveal a stable tridentate coordination of the Mg^{2+} by GTP in water, and a stable bidentate coordination by GTP in complex with Ras. For validation, we compare the calculated frequencies and isotopic shifts with the experimental results available in the range of 800 cm^{-1} to 1300 cm^{-1}. For the first time we suggest band assignments of the vibrational modes below 800 cm^{-1} by comparison of calculated and experimental spectra.

1. Introduction

Approximately 150 different guanine nucleotide-binding proteins are present in eukaryotic cells where they are responsible for various cellular processes. These include heterotrimeric G-proteins with α, β, and γ subunits, members of the Ras-related superfamily, and others. The signal transduction processes involved in cell growth and differentiation are accomplished with the hydrolysis of guanosine triphosphate (GTP).[1–4] The hydrolysis reaction is initialized by the binding of GTP to the Ras protein. With the help of a GTPase-activating protein (GAP), GTP is hydrolyzed by Ras with one water molecule to yield guanosine diphosphate (GDP) and an inorganic phosphate.[5,6] The complex consisting of the Ras protein bound to the hydrolysis product GDP is inactive and can be reactivated again by exchanging the GDP for another GTP. The cycling of GTP hydrolysis is critical for signal transduction by Ras. A malfunction associated with constitutively active Ras can lead to uncontrolled cell proliferation, which eventually causes tumors.[7,8] Therefore, the mechanisms of GTP hydrolysis have been extensively investigated by a great number of theoretical methods,[9–19] and by experimental techniques such as X-ray crystallography,[20–22] nuclear magnetic resonance spectroscopy,[23] and Fourier-transformed infrared (FTIR) spectroscopy.[24–36]

The technique of FTIR spectroscopy is a versatile tool that can detect the specific vibrations of GTP in proteins at the atomic level.[29] Spectra are sensitive to structural details below the resolution of X-ray crystallography, and can indicate changes in bond length and charge distribution that are otherwise not accessible. Through monitoring the variations of infrared bands with time, we can follow the hydrolysis process proceeding from GTP to GDP on the nanosecond timescale.[30] The variations of specific vibrations with time indicate changes in GTP structure with the cleavage and formation of new chemical bonds.[31] FTIR investigations can therefore reveal reaction mechanisms and allow us to derive reaction rate constants of GTP hydrolysis.[32,33] However, measurements from FTIR spectroscopy usually lack three-dimensional structural information for specific vibrations. To solve this problem, some researchers have resorted to a combination of quantum mechanics and molecular mechanics (QM/MM) methods for studying the spectra of substrates in

[a] *Chinese Academy of Sciences-Max Planck Partner Institute and Key Laboratory for Computational Biology, Shanghai Institutes for Biological Sciences, 320 Yue Yang Road, Shanghai, 200031, China. E-mail: gerwert@bph.rub.de*
[b] *Department of Biophysics, University of Bochum, ND 04 North, 44780 Bochum, Germany*

† Electronic supplementary information (ESI) available. See DOI: 10.1039/c1cp22741f

biological systems.[37–41] For instance, Klähn *et al*. analyzed and structurally assigned the vibrational frequencies, charge distributions, and bond lengths of GTP in the Ras protein and found that the charge transfer effect occurred during the process of GTP hydrolysis.[40] te Heesen *et al*. studied the specific vibrations of the triphosphate moiety of GTP to arrive at an explanation of the role of GAP in activating the P–O bonds of GTP.[41] These investigations have demonstrated that theoretical studies of spectra are of great importance for revealing the mechanisms of biochemical reactions that occur in proteins.

In terms of specific vibrations of GTP in the Ras protein, previous experimental and theoretical studies have focused solely on infrared vibrations above 800 cm^{-1}, and bands below 800 cm^{-1} have not yet been assigned.[27,28,30,32,33] In this study, we report theoretical QM/MM investigations of the low-lying normal vibration modes of GTP in the Ras protein and assign the experimental infrared bands of Ras·GTP·Mg^{2+} in the difference spectrum for the first time. To achieve this, we first verified the QM/MM method used in this study by recalculating the specific vibrations of GTP in the range of approximately 800 to 1300 cm^{-1}. In earlier calculations a relatively small QM region was chosen.[41] It is known that normal mode analysis usually depends on the size and number of chosen atoms. Since the ribose ring might be vibrationally coupled with the triphosphate group, we deemed it better to include the covalently connected ribose ring of GTP in the QM region. We further tried to improve the results by employing the hybrid functional B3LYP[42,43] instead of the Becke–Perdew method.[42,44] The Becke–Perdew method belongs to the category of generalized gradient approximation (GGA) in the density functional theory (DFT). In principal, GGA functionals are less accurate than hybrid functionals in calculations of molecular conformations and energetics, particularly those of the strong electron correlations in phosphoric compounds.[45] Using a high-level DFT functional could therefore improve the accuracy of frequency calculations. Our preliminary calculations in the range of approximately 800 to 1300 cm^{-1} demonstrate the improved accuracy of the B3LYP method. Subsequently, we analyzed theoretical normal vibration modes of frequencies below 800 cm^{-1}, and assigned the infrared bands of Ras·GTP·Mg^{2+} in the difference spectrum by comparison with one another. Our investigations have revealed new specific vibrations of the GTP triphosphate bound to Ras at frequencies below 800 cm^{-1}.

In addition, several problems remain in the assignments of specific vibrations of free GTP and the GTP·Mg^{2+} complex in solution. Previous infrared experiments reported five specific vibrations each for free GTP and the GTP·Mg^{2+} complex, respectively.[25,26] Among these, the antisymmetric normal vibration modes of $\nu_a(PO_2)_\alpha$ and $\nu_a(PO_2)_\beta$, as well as the two $\nu_a(PO_3)_\gamma$ modes, have been assigned with only one frequency value each. However, $\nu_a(PO_2)_\alpha$ and $\nu_a(PO_2)_\beta$ are separated normal vibration modes, and the $(PO_3)_\gamma$ group should possess two antisymmetric $\nu_a(PO_3)_\gamma$ vibrational frequencies. Recently, two additional crucial stretching vibrations, $\nu_s(OP_\beta O)$ and $\nu_a(OP_\beta O)$, associated with the hydrolysis of GTP in the Ras protein, have been detected by FTIR spectroscopy,[30] but no counterparts have yet been reported in the spectra of free GTP and the GTP·Mg^{2+} complex in solution. Therefore, a detailed theoretical analysis of the normal vibration modes of GTP and GTP·Mg^{2+} complex in solution is required to clarify these questions. In this study, we first present the results of molecular mechanics (MM) simulations of GTP, GTP·Mg^{2+}, and Ras·GTP·Mg^{2+} in brief, and then discuss the normal vibration analysis of these complexes in detail, based on QM/MM calculations.

2. Experimental and theoretical methods

2.1 MM simulations

All MM simulations were carried out using optimized potentials for liquid simulations (OPLS) force fields,[46] complemented by optimized GTP parameters, within the Gromacs software package (v3.3.1).[47] The initial atom coordinates of the Ras·GTP·Mg^{2+} complex were taken from the crystal structure deposited in the protein data bank (PDB ID:1QRA).[21] The Ras·GTP·Mg^{2+} complex was immersed in a cubic water box with 20 429 TIP4P water molecules.[48] To mimic physiological salt concentration, 62 sodium cations and 52 chlorine anions were added into the water box to keep the whole system neutral. Similar systems were also set up for the free GTP molecule and the GTP·Mg^{2+} complex. Periodic boundary conditions were applied to the cubic water box and the electronic interactions of the system were evaluated using the Fast Particle-Mesh Ewald method.[49] The van der Waals interactions between atom pairs were truncated within a cutoff value of 1.0 nm. A Berendsen thermostat with a coupling constant of 0.1 ps and a Berendsen barostat with a coupling constant of 1.0 ps were used to keep the system at a constant temperature of 300 K and 1 standard atmosphere, respectively.[50] The system was first energy-minimized and then heated and pre-equilibrated for 5 ns with an integration step of 1 fs to achieve equilibrium. Finally, the 50 ns MM trajectories of each system in equilibrium were analyzed.

2.2 QM/MM simulations

The Gromacs software package (v. 3.3.1) was interfaced with Gaussian03 (G03) for QM/MM simulations.[51,52] The normal QM/MM scheme in the Gromacs package was employed in our study.[53] According to this scheme, the total Hamiltonian $\hat{H}$ of the system is composed of three parts, *i.e.*, $\hat{H} = \hat{H}_{QM} + \hat{H}_{MM} + \hat{H}_{QM/MM}$. The term $\hat{H}_{QM}$ represents a quantum mechanical description of the chosen atoms. In our study, atoms in the QM region were treated using the B3LYP method combined with the 6-31G* basis set, denoted as B3LYP/6-31G*. The term $\hat{H}_{MM}$ represents the MM region, which is described using the parameters of the OPLS force field. The term $\hat{H}_{QM/MM}$ mainly accounts for the electrostatic and VDW interactions between the QM and MM parts. The electrostatic interactions between QM and MM regions were evaluated by treating the MM atoms as point charges when the QM atoms are polarized by the MM atoms.[54] The van der Waals interaction energy between the QM and MM atoms was directly estimated from the parameters of the OPLS force field. Final snapshots were extracted from the MM simulations to set up the QM/MM systems. The QM/MM simulations were extended for 100 ps by reading the coordinates and velocities of the final MM snapshots. Fig. 1 demonstrates the division of the QM/MM regions for GTP, GTP·Mg^{2+}, and Ras·GTP·Mg^{2+}

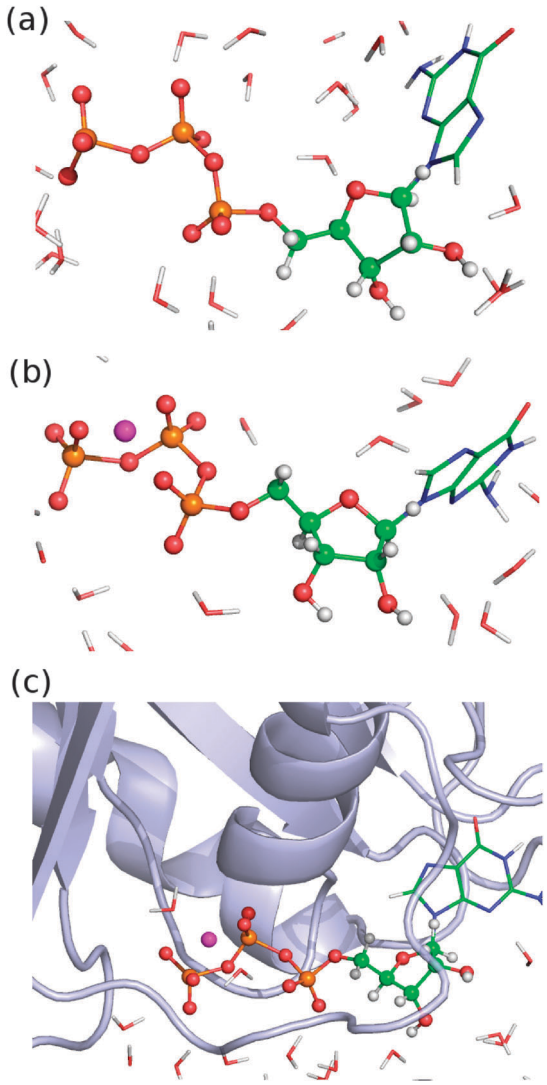

Fig. 1 The QM/MM division of the GTP, GTP·Mg^{2+}, and Ras·GTP·Mg^{2+} systems in solution: the QM atoms are represented by spheres, water molecules by lines and the Ras protein by the cartoon representation. The QM and MM regions of all three systems are divided by cutting the C–N bonds between the ribose rings and guanine bases, where the QM regions are saturated by hydrogen atoms. (a) The QM region of GTP contains the triphosphate group, the ribose ring, and the link atom, and the rest belongs to the MM region. (b) The magenta Mg^{2+} ion of GTP·Mg^{2+} is also included in the QM region, and compared to that of free GTP. (c) The QM region is the same as that of GTP·Mg^{2+}, and the rest is included in the MM region.

systems in solution. The QM region for GTP in solution included the triphosphate group, the ribose ring and the link atom,[55] while the Mg^{2+} ions were also included in the QM regions of GTP·Mg^{2+} and Ras·GTP·Mg^{2+}.

2.3 Normal vibration mode analysis and isotope labeling calculations

Cui and Karplus have proposed a joint QM/MM energy minimization method for normal vibration analysis of molecules in condensed systems.[56] The normal vibration modes of a selected QM region can be obtained by diagonalizing its Hessian matrix after QM/MM energy minimization. Another similar method is the so-called instantaneous normal-mode analysis by which the QM region is minimized by fixing the MM region at the structure at 300 K.[9] Using the joint QM/MM optimization method, it is easier to obtain the normal vibration modes and infrared vibration frequencies of the chosen QM region, which can then be directly compared to available experimental data. Following this method, we extracted a series of snapshots from the first 10 ps of QM/MM trajectories to perform the joint QM/MM energy minimization. The structure was well equilibrated after 2.5 ps of QM/MM simulation, and we observed no differences between snapshots extracted after 2.5 ps, 10 ps, or 100 ps (see Table S1, ESI†). Based on the 2.5 ps optimized structures, we performed the normal mode analysis and obtained the corresponding harmonic vibration frequencies for the triphosphate group of GTP. To carry out isotope labeling calculations, we substituted the ^{16}O atoms in the triphosphate by the isotope ^{18}O to perform the frequency analysis. The vibrational frequency and isotope labeling calculations were carried out at 300 K and 1 standard atmosphere in G03.

2.4 FTIR measurements

Expression and purification of the H-Ras 1–166 protein and FTIR measurements of the same were performed as described before.[57] The sample solution for FTIR measurements contained 10 mM Ras 1–166, 200 mM MES (pH 6.0), 20 mM $MgCl_2$, 20 mM DTT, and 0.1% glycol. Ras was loaded with the P3-1-(2-nitrophenyl)ethyl ester of GTP (caged-GTP). The difference spectrum between Ras·caged-GTP and Ras·GTP was obtained by subtracting spectra collected before from spectra collected after flashing the sample with a XeCl excimer laser. To access the spectrum at low wavenumbers, a liquid helium cooled Si : B detector (IRLabs, Tucson AZ, USA) was used.

3. Results and discussion

3.1 Structural characteristics

To summarize the conformational features of GTP and its complex in condensed phases, we defined two dihedrals associated with the flexibility of the triphosphate. As shown in Fig. 2(a), the two dihedrals Ψ_1 and Ψ_2 were defined in the sequence of the four atoms P_γ–O–P_β–O and O–P_β–O–P_α along the triphosphate group. The dihedral Ψ_1 describes the rotational motion of the $(PO_3)_\gamma$ group around the O–P_β bond, relative to the $(PO_2)_\beta$ group. The dihedral Ψ_2 describes the motion of $(PO_2)_\beta$ relative to the $(PO_2)_\alpha$ group around the P_β–O bond axis. Fig. 2(b) shows the statistical two-dimensional dihedral distributions of GTP, GTP·Mg^{2+}, and Ras·GTP·Mg^{2+} with respect to the coordinates of Ψ_1 and Ψ_2 during MM simulations. Obviously, the Ψ_1 distribution of free GTP varies between $-60°$ and $-180°$, and between $180°$ and $60°$, while those of GTP·Mg^{2+} and Ras·GTP·Mg^{2+} mostly lie in the ranges of approximately $60°$ to $120°$ and $90°$ to $150°$. The dihedral distributions are in accordance with the fact that the backbone of free GTP in solution is more flexible, while the conformations of GTP·Mg^{2+} and Ras·GTP·Mg^{2+} are more restrained due to the coordination of the Mg^{2+} and the Ras protein.

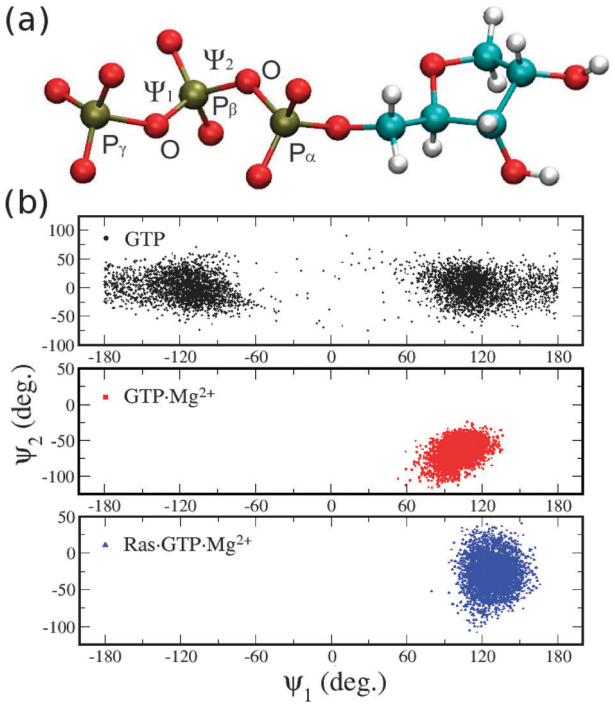

Fig. 2 Flexibility of GTP: (a) The dihedrals Ψ_1 and Ψ_2 are defined by the four sequential atoms P_γ–O–P_β–O and O–P_β–O–P_α along the backbone of triphosphate group, as shown in the scheme. (b) The dihedral distributions of the GTP, GTP in the GTP·Mg^{2+}, and Ras·GTP·Mg^{2+} complexes with respect to the coordinates of Ψ_1 and Ψ_2. The dihedral samples of the GTP, GTP·Mg^{2+}, and Ras·GTP·Mg^{2+} are expressed by black circles, red squares, and blue triangles, respectively, in a total of 5000 points each from their 50 ns MM simulations.

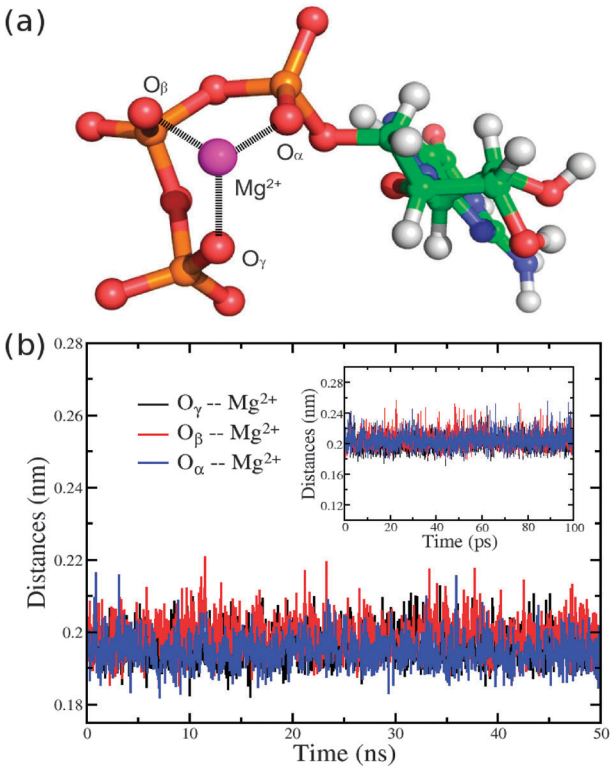

Fig. 3 Mg^{2+} coordination: (a) a snapshot of the structure of GTP·Mg^{2+} in solution, showing that the three oxygen atoms O_γ, O_β, and O_α form strong electrostatic interactions with the Mg^{2+} ion. (b) The monitored distances between the O_γ, O_β, O_α, and Mg^{2+} atom indicate the GTP·Mg^{2+} complex has a stable tridentate coordination. The inset shows similar results obtained from the 100 ps QM/MM simulation.

The experiments reveal that the antisymmetric vibrations of $(PO_2)_{\alpha,\beta}$ and $(PO_3)_\gamma$ groups in the GTP·Mg^{2+} complex are upshifted to 1247 cm^{-1} and 1128 cm^{-1}, compared to 1233 cm^{-1} and 1119 cm^{-1} in free GTP.[25] A conformation of the GTP·Mg^{2+} complex in solution extracted from the MM simulation is shown in Fig. 3(a), where the Mg^{2+} cation is in tridentate coordination with the triphosphate group. The MM simulation of GTP·Mg^{2+} indicates that such a tridentate conformation is quite stable for up to 50 ns, agreeing with previous experimental measurements.[25] As shown in Fig. 3(b), the tridentate coordination is characterized by equidistant interactions between the Mg^{2+} and the O_γ, O_β, and O_α atoms; this is in accordance with the results of QM/MM simulations shown in the inset. The strong electrostatic interactions between these atoms and the Mg^{2+} ion not only result in the upshifting of the antisymmetric vibrations of $\nu_a(PO_2)_{\alpha,\beta}$ and $\nu_a(PO_3)_\gamma$, but also restrain the motions of the $(PO_2)_{\alpha,\beta}$ and $(PO_3)_\gamma$ groups, thereby restricting the dihedral distributions of Ψ_1 and Ψ_2 of GTP·Mg^{2+} within the narrow ranges of approximately 60° to 130° and approximately −30° to −120°. Similarly, the symmetric vibration mode $\nu_s(PO_3)_\gamma$ of Ras·GTP·Mg^{2+} is shifted to 953 cm^{-1}, as compared to 927 cm^{-1} seen in both free GTP and GTP·Mg^{2+}. In Fig. 4, it can be seen that the GTP adopts a bidentate coordination with the Mg^{2+} ion at the active center of Ras protein. The residue Lys16 of the Ras protein forms a network of hydrogen bonds with GTP to stabilize its conformation by interacting with the $(PO_3)_\gamma$ and $(PO_2)_\beta$ groups.[13] The monitored distances between the atom pairs O_γ and H1, O_β and H2, and O_β and H3 indicate that these hydrogen bonds are quite stable even in a longer timescale. The Ψ_1 dihedral distribution of Ras·GTP·Mg^{2+} lies in the range of approximately 90° to 150°. The bidentate coordination of the Mg^{2+} is also proven by the experimental frequencies. If the coordination of Mg^{2+} would be tridentated the asymmetric stretching vibrations of the α and β phosphate would be closer

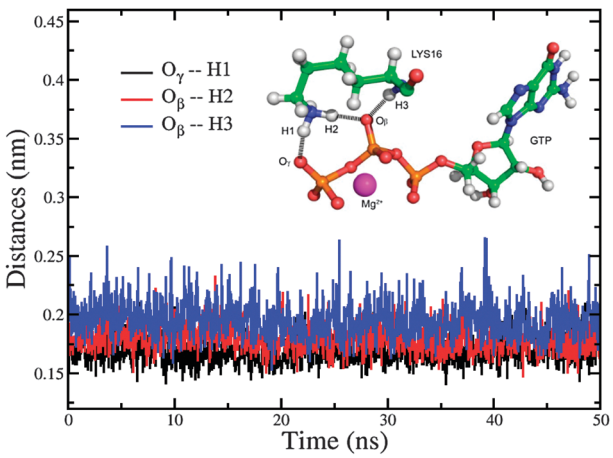

Fig. 4 GTP coordination: monitored distances between the O_γ and O_β oxygen atoms of GTP and the H1, H2, H3 hydrogen atoms of the residue Lys16 in the Ras protein, showing that the conformations of GTP are stabilized by hydrogen bond interactions.

to each other. This can be seen for example in Ran·GTP·Mg^{2+} in which a tridentate coordination of the Mg^{2+} by the GTP occurs.[58] Undoubtedly, the GTP in the Ras protein adopts a particular conformation that is distinctly different from that in the GTP·Mg^{2+} complex, which leads to the difference in their specific vibrations.

3.2 GTP in aqueous solution

In principle, the triphosphate group of GTP has nine normal vibration modes, which are schematically illustrated in Fig. 5. Experimentally, in aqueous solution at pH 7.5,[25] the triphosphate group is composed of a $(PO_2)_\alpha$ group, a $(PO_2)_\beta$ group, and a dianionic $(PO_3)_\gamma$ group. The $(PO_2)_\alpha$ and $(PO_2)_\beta$ groups possess antisymmetric and symmetric stretching vibration modes, denoted as $\nu_{a/s}(PO_2)_\alpha$ and $\nu_{a/s}(PO_2)_\beta$, respectively, while the $(PO_3)_\gamma$ moiety has two antisymmetric vibrations, denoted as $\nu_a(PO_3)_\gamma$, and a symmetric vibration $\nu_s(PO_3)_\gamma$. In spectroscopic experiments,[25] several infrared absorption peaks at wavenumbers 1233 cm^{-1}, 1119 cm^{-1}, 1087 cm^{-1}, and 927 cm^{-1}, and a sharp Raman absorption peak at 1116 cm^{-1}, have been observed for free GTP in solution. The antisymmetric stretching modes of the $(PO_2)_\alpha$ and $(PO_2)_\beta$ groups are expected to appear in the infrared region at approximately 1150 to 1250 cm^{-1}. In fact, a broad infrared band at 1234 cm^{-1} has been observed for adenosine triphosphate (ATP) in solution, which has been attributed to the overlapping of the two vibration modes $\nu_a(PO_2)_\alpha$ and $\nu_a(PO_2)_\beta$.[24] Wang *et al.* also observed a similar band at 1233 cm^{-1} for GTP in solution, with the same conclusion.[25] Our theoretical calculations generated two different frequencies corresponding to the two antisymmetric normal vibration modes. Fig. 6(a) shows all the calculated frequencies for the specific vibrations of the GTP triphosphate compared to the available experimental data of ATP and GTP in solutions of pH 7.0 and 7.5.[24,25] The calculated values appear to have bigger deviations compared to experimental values because GTP in solution is much more flexible, as shown in Fig. 2(b). More snapshots might yield better results in accordance with experimental spectra by taking this heterogeneity into account. However, this has no effect on the normal mode analysis of GTP in solution. The calculated values for $\nu_a(PO_2)_\alpha$ and $\nu_a(PO_2)_\beta$ vibrations were 1258 cm^{-1} and 1236 cm^{-1}, respectively, with only a tiny separation of about 22 cm^{-1} between them. Additional experiments revealed that the symmetric vibration modes of the $(PO_2)_\alpha$ and $(PO_2)_\beta$ groups couple with each other in solution, leading to new in-phase and out-of-phase modes, denoted as $\nu_{in}(PO_2)_{\alpha,\beta}$ and $\nu_{out}(PO_2)_{\alpha,\beta}$.[30] We assigned the experimentally measured absorptions at 1116 and 1087 cm^{-1} to the modes of $\nu_{in}(PO_2)_{\alpha,\beta}$ and $\nu_{out}(PO_2)_{\alpha,\beta}$, respectively. Interestingly, the counterparts of these two vibrations in the ATP spectrum are also located at the wavenumbers 1116 and 1087 cm^{-1}. The QM/MM calculations yield values of 1100 cm^{-1} and 1087 cm^{-1} for the $\nu_{in}(PO_2)_{\alpha,\beta}$

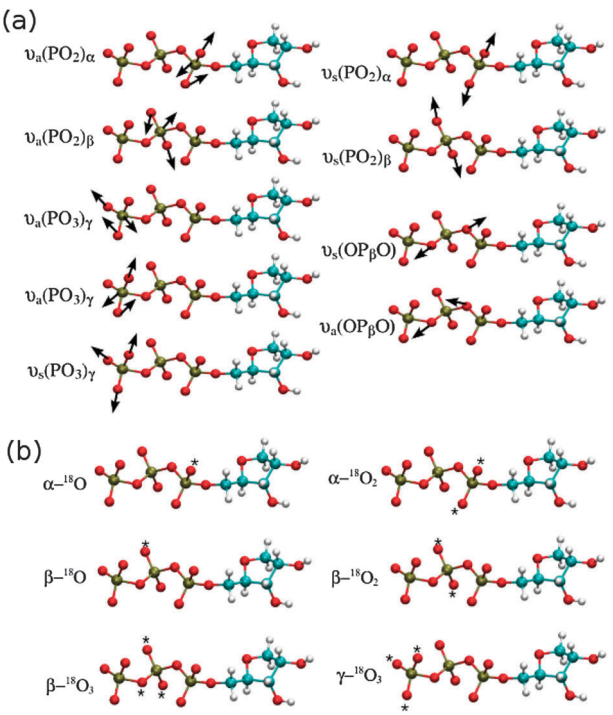

Fig. 5 Stretching normal vibration modes of the triphosphate: The antisymmetric and symmetric vibration modes of $(PO_2)_\alpha$, $(PO_2)_\beta$, and $(PO_3)_\gamma$ groups are denoted as $\nu_a(PO_2)_\alpha$, $\nu_a(PO_2)_\beta$, $\nu_a(PO_3)_\gamma$ and $\nu_s(PO_2)_\alpha$, $\nu_s(PO_2)_\beta$, $\nu_s(PO_3)_\gamma$, respectively. The notations of $\nu_s(OP_\beta O)$ and $\nu_a(OP_\beta O)$ denote the symmetric and antisymmetric stretching vibrations of the O-P_β-O group in the triphosphate.

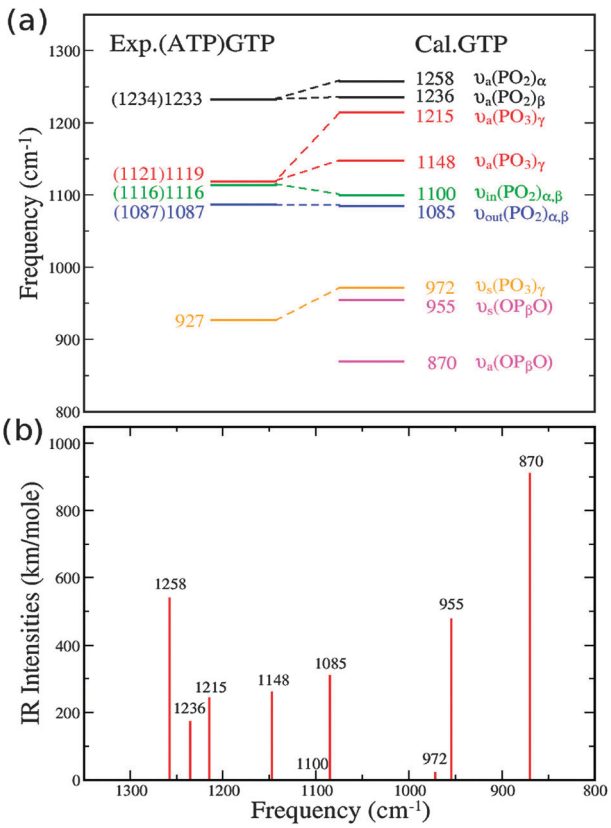

Fig. 6 Vibrations of free GTP in water: (a) Comparison of the experimental values of GTP and the frequencies calculated from the QM/MM simulations for free GTP in water. The specific frequencies of ATP are listed in the parentheses as a reference. The experimental values of ATP and GTP are taken out from previous studies.[24,25] (b) The calculated IR intensities of the normal vibration modes corresponding to (a) are expressed by line lengths.

and $\nu_{out}(PO_2)_{\alpha,\beta}$ coupling vibration modes, respectively, in good agreement with experimental data.

The $(PO_3)_\gamma$ moiety of triphosphate has an approximate C_{3V} symmetry, giving rise to two nearly degenerate antisymmetric $\nu_a(PO_3)_\gamma$ vibrations and a symmetric $\nu_s(PO_3)_\gamma$ vibration. The two antisymmetric vibrations are split into two nondegenerate vibrations due to the breaking of the symmetry of the $(PO_3)_\gamma$ group in solution. Previous experiments only reported one broad infrared band with a peak at 1119 cm^{-1}, which accounts for the $\nu_a(PO_3)_\gamma$ vibration, while the others have not been identified. Our theoretical calculations indicate that the antisymmetric vibrations of the $(PO_3)_\gamma$ group are located at 1148 and 1215 cm^{-1}. Based on the current model, it appears that the calculated value of 1215 cm^{-1} might be slightly overestimated, since the two nearly degenerate antisymmetric vibrations should be only slightly separated, as seen with the two experimental $\nu_a(PO_2)_\alpha$ vibrations of Ras·GTP·Mg^{2+}. The symmetric stretching mode of $\nu_s(PO_3)_\gamma$ has been previously assigned to the vibration at 927 cm^{-1} in the Raman spectrum.[25] However, Takeuchi *et al.* have suggested that the $\nu_s(PO_3)_\gamma$ should be near 1000 cm^{-1}, which is closer to our calculated value of 972 cm^{-1}.[24] Besides these, there are two additional vibration modes of the triphosphate group, the symmetric $\nu_s(OP_\beta O)$ and the antisymmetric $\nu_a(OP_\beta O)$ stretching vibrations that are considered important for the hydrolysis of GTP in solutions. These two vibrations have not been reported for GTP in solution in previous experiments, but their counterpart vibrations have been measured in the Ras·GTP·Mg^{2+} protein complex recently.[30] Our theoretical calculations yielded values of 955 and 870 cm^{-1} for the symmetric $\nu_s(OP_\beta O)$ and the antisymmetric $\nu_a(OP_\beta O)$ vibrations, respectively.

The IR intensities of the nine specific normal vibration modes were calculated based on the current QM/MM models, which provide instructive indications of the strengths of infrared bands observed experimentally.[25] Experimentally, the vibration modes of $\nu_a(PO_2)_{\alpha,\beta}$, $\nu_a(PO_3)_\gamma$, and $\nu_{out}(PO_2)_{\alpha,\beta}$ appear as strong broad bands at 1233, 1119, and 1087 cm^{-1}, while the symmetric stretching modes of $\nu_{in}(PO_2)_{\alpha,\beta}$ and $\nu_s(PO_3)_\gamma$ are relatively weak in the IR spectra. Correspondingly, the calculated intensities of normal vibration modes at 1258 and 1236 cm^{-1} for $\nu_a(PO_2)_{\alpha,\beta}$, 1215 and 1148 cm^{-1} for $\nu_a(PO_3)_\gamma$, and 1085 cm^{-1} for $\nu_{out}(PO_2)_{\alpha,\beta}$ are also quite strong, while the intensities of the two symmetric vibrations at 972 cm^{-1} and 1100 cm^{-1} are almost invisible. Therefore, the calculated intensities of normal vibration modes from the QM/MM models qualitatively indicate the strengths of the experimentally observed infrared bands.

3.3 GTP·Mg^{2+} complex in solution

Fig. 3 demonstrates that MM and QM/MM simulations are consistent with experimental observations of the structure of GTP·Mg^{2+} in solution. MM simulations demonstrate that the GTP forms a stable tridentate coordination with the Mg^{2+} ion in the GTP·Mg^{2+} complex in solution. Further, QM/MM simulations begin with a bidentate structure which finally leads to the tridentate coordination pattern. The strong electrostatic interactions between the triphosphate group and Mg^{2+} ion influence the vibrational strengths of P–O bonds of the triphosphate group. IR experiments have shown that the specific vibrations of these groups are upshifted by several wavenumbers in the presence of the Mg^{2+} cation.[25] For example, the antisymmetric stretching vibration modes of $\nu_a(PO_2)_\alpha$ and $\nu_a(PO_2)_\beta$ upshift from 1233 cm^{-1} to 1247 cm^{-1} when GTP coordinates with the Mg^{2+} cation in solution. Similar to observations with free GTP, only one infrared band was observed around 1247 cm^{-1} in the spectrum of GTP·Mg^{2+}. However, the infrared spectrum of ATP·Mg^{2+} in solution exhibits two separated peaks at wavenumbers 1252 and 1235 cm^{-1}, corresponding to the $\nu_a(PO_2)_\alpha$ and $\nu_a(PO_2)_\beta$ vibrations, respectively.

Fig. 7(a) shows the experimental and calculated frequencies of GTP·Mg^{2+} as well as ATP·Mg^{2+} in solution. We obtained values of 1268 cm^{-1} and 1235 cm^{-1} for the $\nu_a(PO_2)_\alpha$ and $\nu_a(PO_2)_\beta$ vibration of GTP·Mg^{2+}, respectively, quite close to the corresponding values for the ATP·Mg^{2+} complex. The band corresponding to the antisymmetric stretching vibrations of the $\nu_a(PO_3)_\gamma$ group in the GTP·Mg^{2+} complex was upshifted by 9 cm^{-1} to 1128 cm^{-1} relative to that of free GTP, similar to the value of 1130 cm^{-1} measured for the ATP·Mg^{2+} complex. We also estimated values of 1218 and 1139 cm^{-1} for the two antisymmetric $\nu_a(PO_3)_\gamma$ vibration modes, although the 1218 cm^{-1} value might be slightly overestimated. For the GTP·Mg^{2+} complex in solution, the symmetric $\nu_s(PO_2)_\alpha$ and $\nu_s(PO_2)_\beta$ vibrations still couple with each other to yield two new

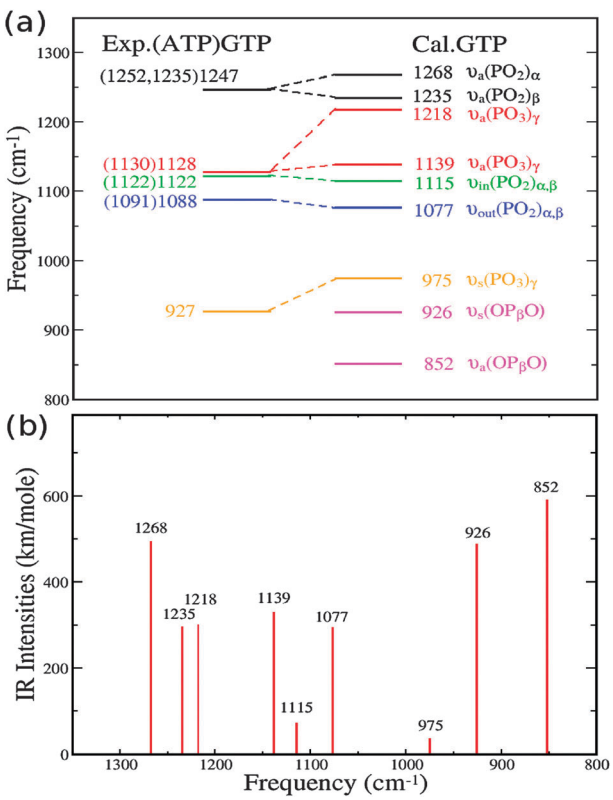

Fig. 7 Vibrations of the GTP Mg^{2+} complex in water: (a) Comparison of experimental values and frequencies calculated from the QM/MM simulations of GTP in the GTP·Mg^{2+} complex in solution. The specific frequencies of ATP in the ATP·Mg^{2+} complex are listed in parentheses as a reference. The experimental values of ATP·Mg^{2+} and GTP·Mg^{2+} are taken out from previous studies.[24,25] (b) The calculated IR intensities of the normal vibration modes corresponding to (a) are expressed by line lengths.

vibration modes, $\nu_{in}(PO_2)_{\alpha,\beta}$ and $\nu_{out}(PO_2)_{\alpha,\beta}$. The calculated frequencies for the above vibration modes are 1115 and 1077 cm^{-1}, respectively, which approach the experimentally determined values of 1122 and 1088 cm^{-1} for GTP·Mg^{2+} as well as the values of 1122 and 1091 cm^{-1} for ATP·Mg^{2+}. The experimentally reported symmetric $\nu_s(PO_3)_\gamma$ vibration remains unchanged at 927 cm^{-1} in the presence of Mg^{2+} cation, and we still predict a higher value of 975 cm^{-1} for this vibration. Comparison of the experimentally reported values of free ATP and GTP, as well as of ATP·Mg^{2+} and GTP·Mg^{2+} complexes in solution, reveals that the specific vibrations of the ATP and GTP triphosphate groups are similar. The two measured values of 1252 and 1235 cm^{-1} for the $\nu_a(PO_2)_\alpha$ and $\nu_a(PO_2)_\beta$ of ATP·Mg^{2+}, respectively, indicate that GTP·Mg^{2+} should have similar vibrational frequencies for the two antisymmetric vibration modes, rather than one value at wavenumber 1247 cm^{-1}, as observed experimentally. We believe that the infrared band with a peak at 1247 cm^{-1} might be regarded as the overlapping of two adjacent infrared bands of the $\nu_a(PO_2)_\alpha$ and $\nu_a(PO_2)_\beta$ vibrations. This is supported by labeling experiments at the $(PO_2)_\beta$ group of the GTP·Mg^{2+} complex. Additionally, values of 926 and 852 cm^{-1} were generated for the symmetric $\nu_s(OP_\beta O)$ and the antisymmetric $\nu_a(OP_\beta O)$ stretching vibrations, respectively.

Fig. 7(b) shows calculated IR intensities corresponding to the normal vibration modes in Fig. 7(a). The strengths of the normal vibration modes at frequencies 1268, 1235, 1139, and 1077 cm^{-1} are as strong as observed in the experimental infrared spectra. The IR strength of the vibration at 1235 cm^{-1} is relatively weak compared to the one at 1268 cm^{-1}; this might be the reason why only one peak at 1247 cm^{-1} has been observed experimentally for GTP·Mg^{2+}. The calculated relative strengths of the vibrations at 1268 and 1235 cm^{-1} are also consistent with the experimental observations of infrared peaks at 1252 and 1235 cm^{-1} in the spectrum of ATP·Mg^{2+}. The less strong vibration of 1077 cm^{-1} is visible next to the vibration of 1139 cm^{-1}, analogous to corresponding experimental observations in the spectrum of the GTP·Mg^{2+} complex.

3.4 GTP bound to Ras protein

The specific vibration frequencies of GTP in the Ras protein were calculated in a previous study by Klähn *et al.*[40] Their results predicted almost correctly the experimentally observed order of spectral bands of GTP, with the exception of one antisymmetric mode, which was redshifted. te Heesen *et al.* obtained more accurate calculation results with a relative deviation of 3.2% from the experimental data.[41] Our QM/MM calculations have further improved the calculated infrared spectra of the Ras·GTP·Mg^{2+} complex in solution. A comparison of experimental spectra and calculated frequencies of the Ras·GTP·Mg^{2+} complex is shown in Fig. 8(a). All nine calculated results are in good agreement with the experimental values. To further compare our values with previous QM/MM results, we evaluated the average frequencies based on different conformations. As shown in Table S1 (ESI†), the average absolute deviation of previous calculations is 28.1 cm^{-1}, while ours is 20.9 cm^{-1}. Frequencies calculated from the snapshot also exhibit a large improvement compared to experiments. These results demonstrate that the current QM/MM method has an improved accuracy for spectrum calculations. We were therefore able to make use of theoretical calculations to aid in assigning the infrared bands of the Ras·GTP·Mg^{2+} complex below 800 cm^{-1}. The low-lying vibrations are of particular interest because a few important vibrations reflecting the hydrolysis of GTP exist near or below 800 cm^{-1}. Recently, Kötting *et al.* reported values of 895 cm^{-1} and 878 cm^{-1} for the stretching vibrations $\nu_s(OP_\beta O)$ and $\nu_a(OP_\beta O)$, respectively;[30] these vibrations are closely related to the cleavage of the P_γ–O bond in the hydrolysis of GTP, and are considered crucial for detecting the hydrolysis of GTP to GDP in the FTIR spectra. In addition, further hydrolysis of GTP and ATP, which involves the cleavage of other P–O bonds and leads to GMP and AMP as the product, respectively, is very common in the cell.[59,60] This prompted us to explore additional stretching vibrations associated with the hydrolysis of the backbone of GTP.

As shown in Fig. 8(b), we calculated the IR intensities corresponding to the normal vibration modes of the Ras·GTP·Mg^{2+} complex that are represented in Fig. 8(a). Because the calculated IR intensities can provide significant preliminary information about specific vibrations, we used them to explain the experimental difference spectrum shown in Fig. 8(c). The vibrations between 800 cm^{-1} and 1300 cm^{-1} in the difference spectrum have been identified in previous studies,[32,33] but the infrared bands below 800 cm^{-1} have not been assigned since these signals are relatively weak compared to those beyond 800 cm^{-1}. We assigned the infrared bands below 800 cm^{-1} in Fig. 8(c) according to our theoretical calculations. First, we found that three relatively stronger bands appear at 767, 715, and 698 cm^{-1} in the difference spectrum. Fig. 8(b) shows a strong normal vibration mode at 787 cm^{-1}, next to the antisymmetric mode of $\nu_a(OP_\beta O)$ at 878 cm^{-1}. The vibration at 787 cm^{-1} corresponds to the stretching vibration of the P_α–O_α bond, as shown by the arrow in Fig. 8(d). We denoted the stretching mode as $\nu_s(PO)_\alpha$ and assigned it to the infrared band at 767 cm^{-1}. Next, we identified a normal vibration mode at 706 cm^{-1} that represents a symmetric stretching vibration of the backbone P_β–O–P_α, denoted as $\nu_s(P_\beta OP_\alpha)$. This symmetric stretching vibration is important for the study of hydrolysis of GTP to GMP. On the left of the wavenumber 706 cm^{-1}, the calculated mode at 671 cm^{-1} was identified as a bending vibration ν_{b1}. The two stronger signals in the difference spectrum appear to be at 715 and 698 cm^{-1}, corresponding to theoretical vibrations at 706 and 671 cm^{-1}. The bending vibration mode ν_{b1} is very complicated as it involves the collective motions of atoms on the triphosphate. We further theoretically identified additional low-lying bending vibrations of ν_{b2}, ν_{b3}, and ν_{b4} at 580, 570, and 557 cm^{-1}, as shown in Fig. 8(b). It is very interesting to note that in the difference spectrum, three consecutive bands also appear at 584, 574 and 563 cm^{-1}, which could be attributed to the bending vibrations of ν_{b2}, ν_{b3}, and ν_{b4}. Additional supporting information is provided in Table S1 (ESI†). We obtained the same low-lying normal vibration modes below 800 cm^{-1} using different snapshots for our calculations. The proposed new assigned bands might overlap with bands corresponding to amino acids in the experimental data, such as the bands of tyrosine seen in the same region. This can be clarified by labeling experiments.

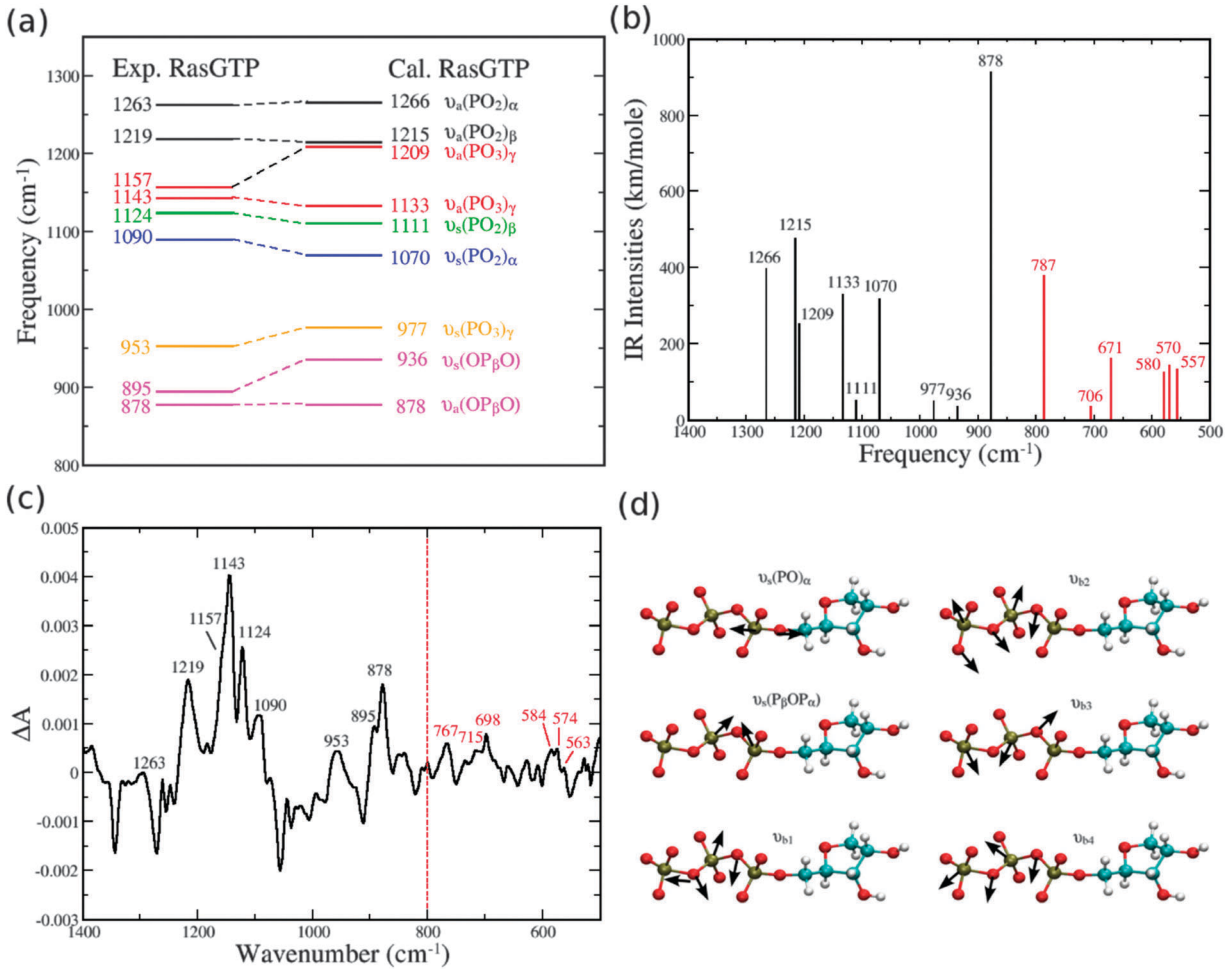

Fig. 8 Vibrations of the GTP Mg^{2+} complex bound to Ras: (a) Comparison of experimental values and calculated frequencies of GTP in the solvated Ras protein. (b) Calculated IR intensities of all normal vibration modes are expressed as line lengths; those below 800 cm^{-1} are in red and above 800 cm^{-1} in black. (c) The experimental difference spectrum between Ras·GTP·Mg^{2+} and Ras·cagedGTP·Mg^{2+} in solutions. The positive bands denote the generation of Ras·GTP·Mg^{2+}. Previously reported bands are labeled in black and new ones below 800 cm^{-1} are labeled in red. (d) The six low-lying vibration modes of the triphosphate group. $\nu_s(PO)_\alpha$ denotes the stretching vibration of the P_α–O_α bond. $\nu_s(P_\beta OP_\alpha)$ denotes the symmetric stretching vibration of P_β–O–P_α bonds. ν_{b1}, ν_{b2}, ν_{b3}, and ν_{b4} denote the bending vibrations of the triphosphate backbone.

3.5 Isotope labeling calculations

The results of isotope labeling calculations are shown in Table 1; the labeling positions refer to the corresponding experiments. For free GTP and GTP·Mg^{2+} complex, we mainly focus on the discussion of labeling calculations of the vibration modes $\nu_a(PO_2)_{\alpha,\beta}$ and $\nu_a(PO_3)_\gamma$, because the experiments only detected one broad band for each of them. The $\nu_a(PO_2)_{\alpha,\beta}$ band at 1233 cm^{-1} can be considered an overlap of two separate bands. The experimental β-$^{18}O_3$ labeling of the triphosphate in GTP results in the shifting of the $\nu_a(PO_2)_{\alpha,\beta}$ vibration from 1233 cm^{-1} to 1220 and 1190 cm^{-1}, respectively. Similarly for the GTP·Mg^{2+} complex, two $\Delta\beta$ Exp values are observed with β-$^{18}O_3$ labeling. In fact, it has been reported that the unlabeled infrared bands corresponding to the $\nu_a(PO_2)_\alpha$ and $\nu_a(PO_2)_\beta$ vibrations of the ATP·Mg^{2+} complex are located at 1252 and 1235 cm^{-1}.[24] With β-$^{18}O_3$ labeling, the two bands shift to 1230 and 1200 cm^{-1}, respectively. The respective shifts are 22 and 35 cm^{-1}, similar to our calculated values of 24 and 14 cm^{-1} for the GTP·Mg^{2+} complex. The antisymmetric vibration $\nu_a(PO_3)_\gamma$ of GTP shifts down by 37 cm^{-1}, to 1082 cm^{-1}, upon γ-$^{18}O_3$ labeling at the $(PO_3)_\gamma$ moiety. We obtained two theoretical values, 34 and 35 cm^{-1}, for this shift. The corresponding value in the GTP·Mg^{2+} complex is 40 cm^{-1}, for which the calculations yield values of 36 and 50 cm^{-1}. Calculations based on both isotope β and γ labeling for free GTP as well as the GTP·Mg^{2+} complex are in agreement with experimentally determined values. For the Ras·GTP·Mg^{2+} system, we compared our isotope calculations with a large volume of available experimental data.[27,33] All the calculated results agree very well with experimental observations. The comparison of the α-^{18}O, β-^{18}O, and γ-$^{18}O_3$ labeling calculations with previous experimental observations[33] indicates that there are no strong vibrational coupling effect between these antisymmetric vibrations. Comparison of our calculations with the observations of Du *et al.*[27] also supports this point. However, there are slight coupling effects between the $(PO_2)_\alpha$ and $(PO_2)_\beta$ groups for the symmetric $\nu_s(PO_2)_\alpha$ and $\nu_s(PO_2)_\beta$ vibrations.

Table 1 Comparison of the isotope unlabeled and labeled frequencies of experiments and calculations

GTP

Modes	Exp.[25]	Cal.	Δα Exp.	Δα Cal.	Δβ Exp.	Δβ Cal.	Δγ Exp.	Δγ Cal.
$\nu_a(PO_2)_{\alpha,\beta}$	1233	1258		4	13	13	4	1
		1236		32	43	15		0
$\nu_a(PO_2)_\gamma$	1119	1215		0		9	37	35
		1148		0		0		34
$\nu_{in}(PO_2)_{\alpha,\beta}$	1116	1100		6	14	7	0	0
$\nu_{out}(PO_2)_{\alpha,\beta}$	1087	1085		29	27	30	0	0

GTP·Mg^{2+}

Modes	Exp.[25]	Cal.	Δα Exp.	Δα Cal.	Δβ Exp.	Δβ Cal.	Δγ Exp.	Δγ Cal.
$\nu_a(PO_2)_{\alpha,\beta}$	1247	1268		33	13	24	3	0
		1235		2	45	14		0
$\nu_a(PO_2)_\gamma$	1128	1218		0		0	40	36
		1139		2		1		50
$\nu_{in}(PO_2)_{\alpha,\beta}$	1122	1115		22	15	31	1	3
$\nu_{out}(PO_2)_{\alpha,\beta}$	1088	1077		37	23	24	0	0

Ras·GTP·Mg^{2+}

Modes	Exp.[33]	Cal.	Δα Exp.	Δα Cal.	Δβ Exp.	Δβ Cal.	Δγ Exp.	Δγ Cal.
$\nu_a(PO_2)_\alpha$	1263	1266	20	21	0	1	0	0
$\nu_a(PO_2)_\beta$	1219	1215	3	1	19	10	1	1
$\nu_a(PO_3)_\gamma$	1157	1209	0	0	0	0	40	35
$\nu_a(PO_3)_\gamma$	1143	1133	1	0	1	0	37	21

Modes	Exp.[27]	Cal.	Δα Exp.	Δα Cal.	Δβ Exp.	Δβ Cal.	Δγ Exp.	Δγ Cal.
$\nu_a(PO_2)_\alpha$	1263	1266	47	35	0	0	0	0
$\nu_a(PO_2)_\beta$	1216	1215	0	2	33	35	1	1
$\nu_a(PO_3)_\gamma$	1158	1209	0	0	0	0	20	35
$\nu_a(PO_3)_\gamma$	1142	1133	0	0	1	2	24	35
$\nu_s(PO_2)_\beta$	1124	1111	15	18	13	35	18	33
$\nu_s(PO_2)_\alpha$	1090	1070	18	20	30	25	1	4
$\nu_s(OP_\beta O)$	897	936	0	0	42	41	20	12
$\nu_a(OP_\beta O)$	880	878	0	0		27	25	27
$\nu_s(PO)_\alpha$		787		3		1		0
$\nu_s(P_\beta OP_\alpha)$		706		5		15		4
ν_{b1}		671		0		16		13
ν_{b2}		580		1		10		10
ν_{b3}		570		2		7		9
ν_{b4}		557		1		17		7

The vibration normal modes are shown in the first column. The labels Exp and Cal indicate the unlabeled experimental frequencies and the values of theoretical calculation results. The Δα, Δβ, and Δγ Exp are experimental vibration shifts with labels at the $(PO_2)_\alpha$, $(PO_2)_\beta$ and $(PO_3)_\gamma$ groups, respectively. The Δα, Δβ, and Δγ Cal are the corresponding calculated values. Previous isotope experiments were carried out by labeling β-$^{18}O_3$ and γ-$^{18}O_3$,[25] as well as by labeling α-^{18}O, β-^{18}O, and γ-$^{18}O_3$,[33] or α-$^{18}O_2$, β-^{18}O, and γ-$^{18}O_4$.[27] All values are in the units of cm^{-1}.

In addition, we calculated the theoretical shift values for all the low-lying vibrations, which can be considered the fingerprints of labeling experiments.

4. Conclusion

We performed simulations of GTP, GTP·Mg^{2+}, and Ras·GTP·Mg^{2+} in solution with physiological sodium chloride concentration. First, the system was preequilibrated using MM and equilibrated using a QM/MM technique. The resulting structures were energy minimized using QM/MM to calculate the spectra by normal mode analysis. With regard to structure, the MM and QM/MM simulations revealed a stable tridentate coordination of the Mg^{2+} by GTP in water and a stable bidentate coordination by GTP in complex with Ras, as expected.

For the first time we assigned the bands below 800 cm^{-1} of the measured FT-IR spectra of the Ras·GTP·Mg^{2+} complex that have remained experimentally undetermined thus far. We also predicted isotopic shifts for these bands. A reliable theoretical assignment was enabled by the agreement of the calculated frequencies and isotopic shifts with the experimentally assigned bands in the range of 800 cm^{-1} to 1300 cm^{-1}. In the Ras·GTP·Mg^{2+} complex, the frequencies deviate only by 19 cm^{-1} on average.

For free GTP and the GTP·Mg^{2+} complex in solution, experimentally one broader band around 1230 cm^{-1} till 1250 cm^{-1} is observed. Here, we found in this region at least two modes, the antisymmetric $\nu_a(PO_2)_{\alpha,\beta}$ and $\nu_a(PO_3)_\gamma$ one. They were separated by 22 cm^{-1} to 33 cm^{-1}. Experimental proof of these values will be pursued in future investigations.

In summary, we show that the combination of QM/MM calculations with vibrational spectroscopy can reveal properties that are not accessible by experimental techniques alone.

Acknowledgements

We thank Yan Suveyzdis for providing the difference spectrum, the Fund for Young Talents Frontier Project (2011KIP310), Shanghai Institutes for Biological Sciences and the Deutsche Forschungsgemeinschaft for financial support (SFB642).

References

1 L. Wiesmüller and F. Wittinghofer, *Mini rev. Cell. Signalling*, 1994, **6**, 247–267.
2 F. McCormick and A. Wittinghofer, *Curr. Opin. Biotechnol.*, 1996, **7**, 449–456.
3 I. R. Vetter and A. Wittinghofer, *Science*, 2001, **294**, 1299–1304.
4 H. R. Bourne, D. A. Sanders and F. McCormick, *Nature*, 1990, **348**, 125–132.
5 M. R. Ahmadian, P. Stege, K. Scheffzek and A. Wittinghofer, *Nat. Struct. Biol.*, 1997, **4**, 686–689.
6 H. R. Bourne, D. A. Sanders and F. McCormick, *Nature*, 1991, **349**, 117–127.
7 R. Mittal, M. R. Ahmadian, R. S. Goody and A. Wittinghofer, *Science*, 1996, **273**, 115–117.
8 A. Wittinghofer and H. Waldmann, *Angew. Chem., Int. Ed.*, 2000, **39**, 4193–4214.
9 M. Kläln, G. Mathias, C. Kötting, M. Nonella, J. Schlitter, K. Gerwert and P. Tavan, *J. Phys. Chem. A*, 2004, **108**, 6186–6194.
10 R. Langen, T. Schweins and A. Warshel, *Biochemistry*, 1992, **31**, 8691–8696.
11 T. Schweins, R. Langen and A. Warshel, *Nat. Struct. Biol.*, 1994, **1**, 476–484.
12 T. Schweins and A. Warshel, *Biochemistry*, 1996, **35**, 14232–14243.
13 K. A. Maegley, S. J. Admiraal and D. Herschlag, *Proc. Natl. Acad. Sci. U. S. A.*, 1996, **93**, 8160–8166.
14 J. Florian and A. Warshel, *J. Phys. Chem. B*, 1998, **102**, 719–734.
15 T. M. Glennon, J. Villa and A. Warshel, *Biochemistry*, 2000, **39**, 9641–9651.
16 A. Shurki and A. Warshel, *Proteins*, 2004, **55**, 1–10.
17 I. A. Topol, R. E. Cachau, A. V. Nemukhin, B. L. Grigorenko and S. K. Burt, *Biochim. Biophys. Acta*, 2004, **1700**, 125–136.

18 B. L. Grigorenko, A. V. Nemukhin, I. A. Topol, R. E. Cachau and S. K. Burt, *Proteins: Struct., Funct., Bioinf.*, 2005, **60**, 495–503.
19 B. L. Grigorenko, A. V. Nemukhin, M. S. Shadrina, I. A. Topol and S. K. Burt, *Proteins: Struct., Funct., Bioinf.*, 2007, **66**, 456–466.
20 K. Scheffzek, M. R. Ahmadian, W. Kabsch, L. Wiesmüller, A. Lautwei, F. Schmitz and A. Wittinghofer, *Science*, 1997, **277**, 333–338.
21 A. J. Scheidig, C. Burmester and R. S. Goody, *Structure*, 1999, **7**, 1311–1324.
22 D. J. Graham, P. N. Lowe, G. W. Grime, M. Marsh, K. Rittinger, S. J. Smerdon, S. J. Gamblin and J. F. Eccleston, *Chem. Biol.*, 2002, **9**, 375–381.
23 M. Rohrer, T. F. Prisner, O. Brugmann, H. Kass, M. Spoerner, A. Wittinghofer and H. R. Kalbitzer, *Proc. Natl. Acad. Sci. U. S. A.*, 2001, **98**, 4944–4949.
24 H. Takeuchi, H. Murata and I. Harada, *J. Am. Chem. Soc.*, 1988, **110**, 392–397.
25 J. H. Wang, D. G. Xiao, H. Deng, R. Callender and M. R. Webb, *Biospectroscopy*, 1998, **4**, 219–227.
26 J. H. Wang, D. G. Xiao, H. Deng, M. R. Webb and R. Callender, *Biochemistry*, 1998, **37**, 11106–11116.
27 X. Du, H. Frei and S. Kim, *J. Biol. Chem.*, 2000, **275**, 8492–8500.
28 H. Cheng, S. Sukal, H. Deng, T. S. Leyh and R. Callender, *Biochemistry*, 2001, **40**, 4035–4043.
29 F. Garczarek and K. Gerwert, *Nature*, 2006, **439**, 109–112.
30 C. Kötting, M. Blessenohl, Y. Suveyzdis, R. S. Goody, A. Wittinghofer and K. Gerwert, *Proc. Natl. Acad. Sci. U. S. A.*, 2006, **103**, 13911–13916.
31 C. Allin, M. R. Ahmadian, A. Wittinghofer and K. Gerwert, *Proc. Natl. Acad. Sci. U. S. A.*, 2001, **98**, 7754–7759.
32 V. Cepus, A. J. Scheidig, R. S. Goody and K. Gerwert, *Biochemistry*, 1998, **37**, 10263–10271.
33 C. Allin and K. Gerwert, *Biochemistry*, 2001, **40**, 3037–3046.
34 P. P. Chakrabarti, Y. Suveyzdis, A. Wittinghofer and K. Gerwert, *J. Biol. Chem.*, 2004, **279**, 46226–46233.
35 C. Kötting and K. Gerwert, *Chem. Phys.*, 2004, **307**, 227–232.
36 C. Kötting, A. Kallenbach, Y. Suveyzdis, A. Wittinghofer and K. Gerwert, *Proc. Natl. Acad. Sci. U. S. A.*, 2008, **105**, 6260–6265.
37 S. Hayashi, E. Tajkhorshid, E. Pebay-Peyroula, A. Royant, E. M. Landau, J. Navarro and K. Schulten, *J. Phys. Chem. B*, 2001, **105**, 10124–10131.
38 R. Rajamani and J. L. Gao, *J. Comput. Chem.*, 2002, **23**, 96–105.
39 R. Rousseau, V. Kleinschmidt, U. W. Schmitt and D. Marx, *Angew. Chem., Int. Ed.*, 2004, **43**, 4804–4807.
40 M. Klähn, J. Schlitter and K. Gerwert, *Biophys. J.*, 2005, **88**, 3829–3844.
41 H. te Heesen, K. Gerwert and J. Schlitter, *FEBS Lett.*, 2007, **581**, 5677–5684.
42 A. D. Becke, *J. Chem. Phys.*, 1993, **99**, 3898–3905.
43 C. Lee, W. Yang and R. G. Parr, *Phys. Rev. B*, 1988, **37**, 785–789.
44 J. P. Perdew, *Phys. Rev. B*, 1986, **33**, 8822–8824.
45 W. Koch and M. C. Holthausen, *A Chemist's Guide to Density Functional Theory*, Wiley-VCH, Second edn, 2001.
46 W. L. Jorgensen, J. Chandrasekhar, J. D. Madura, R. W. Impey and M. L. Klein, *J. Chem. Phys.*, 1983, **79**, 926–935.
47 E. Lindahl, B. Hess and D. van der Spoel, *J. Mol. Mod.*, 2001, **7**, 306–317.
48 W. L. Jorgensen and C. Jenson, *J. Chem. Comput.*, 1998, **19**, 1179–1186.
49 T. Darden, D. York and L. Pedersen, *J. Chem. Phys.*, 1993, **98**, 10089–10092.
50 H. J. C. Berendsen, J. P. M. Postma, A. DiNola and J. R. Haak, *J. Chem. Phys.*, 1984, **81**, 3684–3690.
51 G. Groenhof, M. Bouxin-Cademartory, B. Hess, S. P. de Visser, H. J. C. Berendsen, M. Olivucci, A. E. Mark and M. A. Robb, *J. Am. Chem. Soc.*, 2004, **126**, 4228–4233.
52 M. J. Frisch, G. W. Trucks, H. B. Schlegel, G. E. Scuseria, M. A. Robb, J. R. Cheeseman, J. A. Montgomery, Jr, T. Vreven, K. N. Kudin, J. C. Burant, J. M. Millam, S. S. Iyengar, J. Tomasi, V. Barone, B. Mennucci, M. Cossi, G. Scalmani, N. Rega, G. A. Petersson, H. Nakatsuji, M. Hada, M. Ehara, K. Toyota, R. Fukuda, J. Hasegawa, M. Ishida, T. Nakajima, Y. Honda, O. Kitao, H. Nakai, M. Klene, X. Li, J. E. Knox, H. P. Hratchian, J. B. Cross, V. Bakken, C. Adamo, J. Jaramillo, R. Gomperts, R. E. Stratmann, O. Yazyev, A. J. Austin, R. Cammi, C. Pomelli, J. W. Ochterski, P. Y. Ayala, K. Morokuma, G. A. Voth, P. Salvador, J. J. Dannenberg, V. G. Zakrzewski, S. Dapprich, A. D. Daniels, M. C. Strain, O. Farkas, D. K. Malick, A. D. Rabuck, K. Raghavachari, J. B. Foresman, J. V. Ortiz, Q. Cui, A. G. Baboul, S. Cliord, J. Cioslowski, B. B. Stefanov, G. Liu, A. Liashenko, P. Piskorz, I. Komaromi, R. L. Martin, D. J. Fox, T. Keith, M. A. Al-Laham, C. Y. Peng, A. Nanayakkara, M. Challacombe, P. M. W. Gill, B. Johnson, W. Chen, M. W. Wong, C. Gonzalez and J. A. Pople, *GAUSSIAN 03 (Revision C.02)*, Gaussian, Inc., Wallingford CT, 2004.
53 A. Warshel and M. J. Levitt, *J. Mol. Biol.*, 1976, **103**, 227–249.
54 G. G. Hall and C. M. Smith, *Int. J Quantum Chem.*, 1984, **25**, 881–890.
55 M. J. Field, P. A. Bash and M. Karplus, *J. Comput. Chem.*, 1990, **11**, 700–733.
56 Q. Cui and M. Karplus, *J. Chem. Phys.*, 2000, **112**, 1133–1149.
57 C. Kötting, A. Kallenbach, Y. Suveyzdis, C. Eichholz and K. Gerwert, *ChemBioChem*, 2007, **8**, 781.
58 S. Brucker, K. Gerwert and C. Kötting, *J. Mol. Biol.*, 2010, **401**, 1–6.
59 A. Ghosh, G. J. K. Praefcke, L. Renault, A. Wittinghofer and C. Herrmann, *Nature*, 2006, **440**, 101–104.
60 H. Rehmann, J. Das, P. Knipscheer, A. Wittinghofer and J. L. Bos, *Nature*, 2006, **439**, 625–628.

